Published online 30 January 2019 *Nucleic Acids Research, 2019, Vol. 47, No. 6* **2871–2883**
doi: 10.1093/nar/gkz022

Evidence for a bind-then-bend mechanism for architectural DNA binding protein yNhp6A

Manas Kumar Sarangi[1,†], Viktoriya Zvoda[1,†], Molly Nelson Holte[2], Nicole A. Becker[2], Justin P. Peters[2], L. James Maher, III[2,*] and Anjum Ansari[1,3,*]

[1]Department of Physics, University of Illinois at Chicago, Chicago, IL 60607, USA, [2]Department of Biochemistry and Molecular Biology, Mayo Clinic College of Medicine and Science, Rochester, MN 55905, USA and [3]Department of Bioengineering, University of Illinois at Chicago, Chicago, IL 60607, USA

Received June 21, 2016; Revised December 18, 2018; Editorial Decision January 03, 2019; Accepted January 18, 2019

ABSTRACT

The yeast Nhp6A protein (yNhp6A) is a member of the eukaryotic HMGB family of chromatin factors that enhance apparent DNA flexibility. yNhp6A binds DNA nonspecifically with nM affinity, sharply bending DNA by >60°. It is not known whether the protein binds to unbent DNA and then deforms it, or if bent DNA conformations are 'captured' by protein binding. The former mechanism would be supported by discovery of conditions where unbent DNA is bound by yNhp6A. Here, we employed an array of conformational probes (FRET, fluorescence anisotropy, and circular dichroism) to reveal solution conditions in which an 18-base-pair DNA oligomer indeed remains bound to yNhp6A while unbent. In 100 mM NaCl, yNhp6A-bound DNA unbends as the temperature is raised, with no significant dissociation of the complex detected up to ∼45°C. In 200 mM NaCl, DNA unbending in the intact yNhp6A complex is again detected up to ∼35°C. Microseconds-resolved laser temperature-jump perturbation of the yNhp6a–DNA complex revealed relaxation kinetics that yielded unimolecular DNA bending/unbending rates on timescales of 500 μs−1 ms. These data provide the first direct observation of bending/unbending dynamics of DNA in complex with yNhp6A, suggesting a bind-then-bend mechanism for this protein.

INTRODUCTION

Double-helical DNA is intrinsically resistant to bending and twisting over distances on the scale of its persistence length [∼150 base pairs; (1)]. Deforming DNA for packaging and looping to bring together distant sites is facilitated by DNA 'softening' (i.e. reduction in bending and twisting persistence lengths) *in vivo* to allow tight DNA bending, kinking, and twisting. Besides DNA compaction by supercoiling and packaging proteins such as histone octamers, small 'architectural' proteins induce transient and sharp DNA bending and twisting to accomplish this softening (1–3). We have been particularly interested in the mechanism of sequence-nonspecific architectural DNA-binding proteins as they increase the apparent flexibility of DNA *in vivo*. Prominent sequence nonspecific examples include bacterial HU (4,5), yeast Nhp6A, Nhp6B (6,7) and HMO1 (8,9), the mitochondrial HM protein (10) and mammalian HMGB1 and HMGB2 (11). We have studied how sequence-nonspecific architectural proteins facilitate tight DNA bending *in vitro* (12–17) and DNA looping by lac repressor in living *Escherichia coli* cells (18–20).

High mobility group B (HMGB) proteins comprise a conserved family of eukaryotic architectural DNA binding proteins. Such proteins typically include one or two homologous 'HMG box' domains of ∼80 amino acids, each of which folds into three alpha-helical segments with an 'L' tertiary structure. Through favorable electrostatic interactions driving ion release from DNA (21–23), minor groove amino acid intercalation (2), and sometimes asymmetric charge neutralization (24), HMGB proteins kink DNA, inducing sharp bends of 70–120°. The *Saccharomyces cerevisiae* single HMG box protein Nhp6A (yNhp6A; Figure 1) is used as a model in the current work.

While the ability of HMGB proteins to deform DNA has long been recognized as biologically crucial (25), three mechanistic aspects of the DNA binding and bending process have remained obscure. First, kinetic studies of DNA binding by HMGB proteins have been puzzling. HMGB protein dissociation rates from DNA appeared to depend

*To whom correspondence should be addressed. Tel: +1 312 996 8735; Fax: +1 312 996 9016; Email: ansari@uic.edu
Correspondence may also be addressed to L. James Maher. Tel: +1 507 284 9041; Email: maher@mayo.edu
†The authors wish it to be known that, in their opinion, the first two authors should be regarded as Joint First Authors.
Present addresses:
Manas Kumar Sarangi, Department of Physics, Indian Institute of Technology, Patna 801103, India.
Justin P. Peters, Department of Chemistry and Biochemistry, University of Northern Iowa, Cedar Falls, IA 50614, USA.

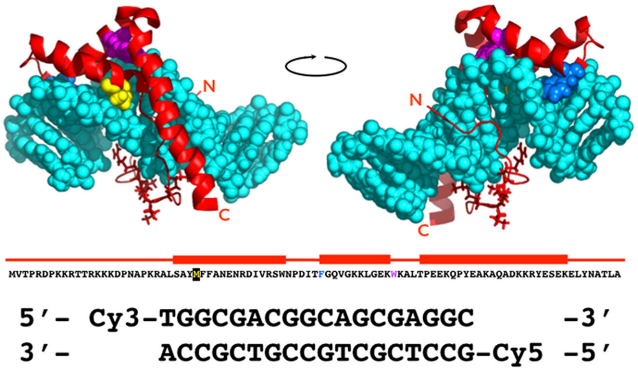

Figure 1. Structure of yNhp6A–DNA complex. NMR structure of yeast HMGB protein Nhp6A (red) bound to duplex DNA (cyan) is shown at the top. The image was created using the Pymol Molecular Graphics System, version 2.0.6 (Schrodinger, LLC) based on PDB structure 1J5N (24). The intercalating methionine, phenylalanine, and tryptophan residues are shown in yellow, blue and magenta, respectively. The amino-acid sequence of the protein is shown with alpha-helical regions indicated by the red rectangles above the amino acid sequence; the intercalating residues are also indicated. The 18-bp oligonucleotide sequence is shown at the bottom, with Cy3 and Cy5 FRET pair attached at the 5′-end of each strand.

on the particular experimental method. Rapid HMGB dissociation rates (~0.1–6 s^{-1}) are observed in bulk experiments in the presence of excess free protein, while dramatically slower rates (10^{-2}–10^{-4} s^{-1}) are observed in the absence of free protein (14,26). This paradox has recently been explained by invoking distinct microscopic and macroscopic protein dissociation modes and a concentration-dependent exchange mechanism between bound and free protein (14,27). A second mechanistic mystery of HMGB protein function is whether the induced DNA deformation is best characterized as a static kink (12,28,29) or a flexible hinge (17). A third mystery of HMGB mechanism is addressed in the present work: the question of whether DNA binding and bending by HMGB proteins are kinetically separable events.

This latter question is illustrated in Figure 2, which shows three possible paths between binding partners (upper left) and product complex with deformed DNA (lower right). The upper 'bend-then-bind' path posits that rare and transient strong DNA bending occurs first, with the deformed DNA captured by random collision with the HMGB protein. The lower 'bind-then-bend' path posits that DNA in a linear conformation is first bound by the HMGB protein, followed by induction or capture of a subsequent bent DNA conformation. The diagonal 'concerted' path reflects the possibility that DNA binding and bending by HMGB proteins might not be kinetically separable events over any time scale. This minimal scheme is not meant to be comprehensive but rather to capture the essence of the current debate in the field as to which pathways are accessible for DNA deformations by DNA-bending proteins. Here we test the hypothesis that the 'bind-then-bend' path (Figure 2) is an available mechanism for HMGB proteins. This key question touches on the fundamental mechanism by which DNA bending is accomplished by architectural proteins, an area illuminated by few experimental results. Understanding the mechanism of DNA deformation for one or more HMGB proteins also may shed light on the roles of HMGB protein domains, notably the characteristic but mysterious N- or C-terminal charged tails in these proteins. Experiments to detect evidence of separable DNA binding and bending steps in HMGB protein mechanism have been limited by the kinetic regimes of available single molecule methods involving optical tweezers (14,17) or fluorescence resonance energy transfer [FRET; (29)]. The time resolution of these approaches has not allowed detection of transient intermediates implied in the upper right or lower left paths of Figure 2, leaving unanswered the question of whether DNA binding and bending can be separable events for HMGB proteins. Experiments with much higher time resolution are required. Here we apply such an approach, rapid temperature-jump (T-jump) kinetics measurements of DNA shape changes by FRET, in concert with an array of equilibrium measurements that monitor the protein–DNA conformations, to probe the mechanism of the single box HMGB protein yNhp6A.

We report spectroscopic experiments examining the thermodynamics and kinetics of DNA binding/bending by purified yNhp6A, when binding without sequence specificity to an 18-base pair DNA duplex. With a combination of FRET, fluorescence anisotropy and circular dichroism (CD) measurements as a function of salt concentration and temperature, we detect for the first time DNA unbending within a stable yNhp6A complex. We apply a nanosecond laser T-jump approach to perturb the yNhp6A–DNA complex and time-resolved FRET to unveil the timescales for DNA bending/unbending in the complex to be in the range of ~500 microseconds to few milliseconds. This study demonstrates that a 'bind-then-bend' pathway is available for yNhp6A, a result previously observed for the structurally unrelated *E. coli* Integration Host Factor (IHF) architectural protein (30–33) as well as for mismatch recognition protein MutS (34), and deduced from free energy simulation studies of binding/bending mechanisms for both Sac7d, a prokaryotic/archaeal DNA packaging protein

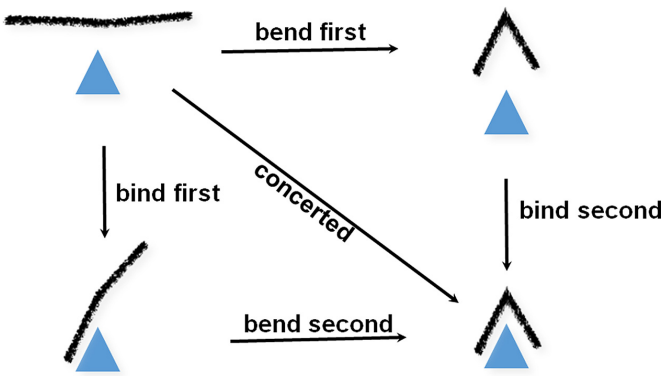

Figure 2. Schematic diagram of DNA binding and bending kinetic pathways. yNhp6A binds free (straight) DNA (upper left) to form a complex in which DNA is bent (lower right). Three possible pathways are shown for the binding/bending: (i) the DNA adopts a bent conformation due to thermal fluctuations and the protein captures the bent conformation (bend-then-bind pathway); (ii) the protein binds to straight DNA with bending in a subsequent step (bind-then-bend pathway); (iii) the binding and bending occurs in a concerted step.

(35), and for RevErbα, a member of the superfamily of nuclear receptors (36).

MATERIALS AND METHODS

DNA preparation

Single-stranded DNA oligonucleotides were purchased from Integrated DNA Technologies (IDT) after synthesis and gel purification. The oligonucleotides were purchased labeled with Cy3 and Cy5 at 5′ termini of complementary strands, as shown in Figure 1. The concentration of each DNA strand and the extent of labeling were determined as described in Supplementary Methods 1.1. Cy3- and Cy5-labeled strands were found to be labeled with 94% and 96% efficiency, respectively. Equimolar concentrations of the upper and lower strands in an annealing buffer (20 mM Tris–HCl, pH 8.0, 500 mM NaCl) were mixed and heated in a water bath at 95°C for 5 min, and then allowed to cool slowly to room temperature for complete annealing.

Protein preparation

Untagged recombinant yNhp6A protein was expressed in bacteria and purified by HPLC as described previously (37). yNhp6A concentration was measured on a Shimadzu UV2101PC7 spectrophotometer applying the Edelhoch method as modified by Pace (38) using an extinction coefficient of 11460 L/mol/cm. This extinction coefficient was determined using the Expasy-protparam tool (https://web.expasy.org/protparam/protparam-doc.html) based on the number of Tyr, Trp and Cys residues in yNhp6A. Protein samples were prepared as described in Supplementary Methods 1.2. All equilibrium and T-jump measurements were carried out in a binding buffer (10 mM HEPES pH 7.5, 1 mM $MgCl_2$, 5% glycerol); the NaCl concentration in the binding buffer was 100, 200 or 300 mM.

Binding measurements from electrophoretic gel mobility shift assays

yNhp6A active concentration and DNA binding stoichiometry were determined for each batch of yNhp6A protein by electrophoretic gel mobility shift assay using 100 nM annealed complementary DNA oligonucleotides 5′-$TG_2CGACG_2CAGCGAG_2C$, and 5′-$GC_2TCGCTGC_2GTCGC_2A$, where the former was first terminally radiolabeled using [γ-^{32}P]-ATP and polynucleotide kinase, and increasing concentrations of yNhp6A, [0, 23, 46, 92, 184, 230, 368, 460, 575, 920 nM and 1.15 μM]. Radiolabeled duplex DNA and yNhp6A were combined in a binding buffer of 10 mM HEPES pH 7.5, 1 mM $MgCl_2$, 7.5% glycerol, 0.24 mg/ml bovine serum albumin at room temperature. Incubation was for 20 min prior to electrophoresis through a 6% 1:19 (w:w) bis:acrylamide native gels in 0.25× TBE buffer at 275 V for 2.25 h. Fraction of total DNA in yNhp6A complex was determined by storage phosphor imaging of dried gels using a Typhoon imager (GE). Estimation of both the dissociation constant, K_D, and unknown active concentration of yNhp6A was accomplished by fitting the experimental values of the fraction of DNA in complex versus protein concentration, as described in Supplementary Methods 1.3.

Binding affinity measurements as a function of salt concentration

Equilibrium dissociation constants for yNhp6A binding to biotinylated 18-bp duplex were estimated as a function of monovalent salt concentration by measuring protein concentration-dependent second-order on-rate and protein concentration-independent first-order off-rate kinetics determined by biolayer interferometry (FortéBIO Octet RED96 instrument). Binding experiments were performed at 25°C in buffer containing 10 mM HEPES pH 7.5, 1 mM $MgCl_2$, 7.5% glycerol, 1 mM DTT, 0.24 mg/ml BSA, 0.02% Tween, at different NaCl concentrations. Details of the measurements and analysis are in Supplementary Methods 1.4.

Thermal stability measurements

Thermal denaturation studies of yNhp6A were performed in 100, 200, or 300 mM NaCl, in the presence and absence of DNA, using far-UV CD measurements at 222 nm, in the temperature range 15–80°C. Measurements were performed on a Jasco J-810 spectropolarimeter, and analyzed in terms of a two-state folding/unfolding transition as described in Supplementary Methods 1.5.

Equilibrium fluorescence measurements

The steady-state fluorescence emission spectra and anisotropies were measured on a FluoroMax4 spectrofluorimeter (HORIBA Scientific). The FRET efficiency between Cy3 (donor) and Cy5 (acceptor) labels in duplex DNA in the absence and presence of yNhp6A protein, and the acceptor ratio (Υ), an equivalent and independent measure of FRET, were determined from the measured spectra as described in Supplementary Methods 1.6. Steady-state anisotropy measurements were performed using acceptor-only labeled samples: Cy5-labeled single-stranded DNA, Cy5-labeled duplex, and Cy5-labeled complex (i.e. duplex in the presence of yNhp6A), as described in Supplementary Methods 1.7. Binding isotherms from acceptor ratio and anisotropy measurements were used to confirm active protein concentrations as described in Supplementary Methods 1.8. Global analysis of the anisotropy data to obtain the fractions of complex, duplex, and single-stranded DNA as a function of temperature is described in Supplementary Methods 1.9.

Laser temperature jump (T-jump) measurements

Rapid T-jump of ∼5–10°C was achieved in sample cuvettes of path length 0.5 mm using ∼10 ns infrared (IR) laser pulse at 1550 nm, and fluorescence emission intensities of the acceptor (Cy5) were measured as a function of time before and after the arrival of the IR pulse, with excitation of the donor (Cy3) accomplished by a continuous wave (cw) laser source at 530 nm. To cover the span of over three orders of magnitude in time, we recorded the T-jump kinetics traces over different timescales and then combined these traces.

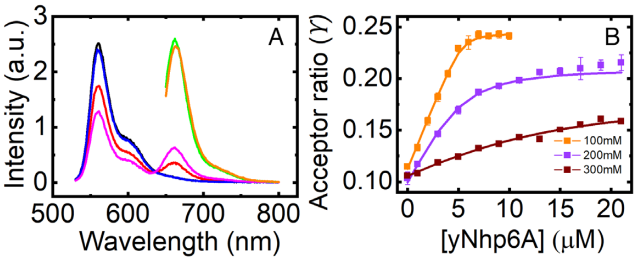

Figure 3. Equilibrium acceptor ratio (Υ) measurements on Cy3–Cy5-labeled yNhp6A–DNA complex. (**A**) The fluorescence emission spectra measured under equilibrium conditions in 100 mM NaCl, with excitation of the donor at 510 nm, are plotted for Cy3-only labeled DNA in the absence (black) and presence (blue) of yNhp6A, and for Cy3–Cy5-labeled DNA in the absence (red) and presence (pink) of yNhp6A. The fluorescence emission spectrum of Cy3–Cy5-labeled DNA, with direct excitation of the acceptor at 645 nm, is also shown in the absence (green) and presence of yNhp6A (orange). (**B**) Acceptor ratio measurements on Cy3–Cy5-labeled DNA as a function of [yNhp6A] at 100 mM NaCl (orange), 200 mM NaCl (indigo), and 300 mM NaCl (burgundy). Measurements were done with 5 μM DNA. The continuous lines are the best fit to a 1:1 binding isotherm, as described in Supplementary Methods 1.8.

The combined traces were analyzed in terms of a single-exponential decay convoluted with another function that described the recovery of the T-jump back to the initial temperature. The details of the laser T-jump spectrometer (31,39,40) and the analysis of the relaxation traces are described in Supplementary Methods 1.10 and 1.11.

RESULTS

To unravel the binding/bending mechanism of yNhp6A–DNA interactions, we performed a series of equilibrium acceptor ratio (Υ) and anisotropy (r) measurements on fluorescently-labeled 18-bp DNA both in the presence and absence of yNhp6A, and corresponding T-jump kinetics measurements, over a range of temperatures and NaCl concentrations ([NaCl]). The equilibrium measurements are presented first, providing the basis for interpretation of the kinetics measurements. Two sets of equilibrium measurements were performed as a function of temperature and salt concentration: FRET (or acceptor ratio) measurements provide information on the change in the extent to which the DNA is bent, whether free or in complex. In contrast, anisotropy measurements detect changes in the fractional population of bound and free DNA, essentially independent of the extent of DNA bending. These measurements, together with circular dichroism (CD) measurements that monitored the folding stability of the protein, free and in complex, provide clear evidence for a 'bind-then-bend' mechanism for yNhp6A, as detailed below.

FRET measurements reveal DNA bending by yNhp6A

Equilibrium FRET measurements are summarized in Figure 3. Typical steady-state emission spectra of Cy3–Cy5 labeled DNA measured at 20°C in the presence and absence of yNhp6A are shown in Figure 3A. The overlapping spectra of Cy3-only labeled DNA in the absence (black curve) and presence of yNhp6A (blue curve) indicate that the quantum yield of the dye attached at the terminus of the duplex DNA is not affected by the binding of the protein. The emission spectrum of Cy3–Cy5 labeled DNA upon excitation of the donor (Cy3) shows a decrease in the donor fluorescence (~560 nm) and a corresponding appearance of the acceptor (Cy5) fluorescence (~660 nm; red curve), indicating FRET between the donor and acceptor dyes at opposite termini of the 18-bp DNA. The FRET efficiency (E) was calculated using the donor fluorescence method as described in Supplementary Methods 1.6. To ensure that un-annealed donor-labeled single strands were not misrepresenting the measured FRET, we carried out these studies for increasing concentration of the acceptor-labeled strands relative to the donor-labeled strands (Supplementary Figure S1). These measurements yield a FRET E value of ~0.3 for the DNA-only sample.

In the presence of yNhp6A, the donor fluorescence is further quenched with a corresponding increase in the acceptor emission (Figure 3A, magenta curve), yielding a higher FRET value of ~0.5. Thus, DNA deformations induced by yNhp6A binding, such as strong DNA bending and likely some DNA twisting as seen in the NMR structure of the yNhp6A–DNA complex (24), are detected as an increase in FRET between the donor and acceptor dyes. These results are in good agreement with single-molecule FRET measurements on identical DNA samples in the presence and absence of the protein, prepared under identical buffer and salt conditions as used in this study (29). This increase in FRET by ~0.2 is also consistent with previously reported FRET changes upon binding by other DNA-bending proteins known to bend DNA to a similar extent (~50–60°), e.g. restriction enzyme EcoRV (41) and DNA mismatch recognition protein MutS (34).

An alternative method for monitoring FRET changes is a measurement of acceptor ratio, defined as the ratio of acceptor emission intensity measured on a double-labeled sample when the donor is excited, to that measured on the same sample when the acceptor is excited directly (42). Figure 3A shows spectra measured from direct excitation of the acceptor in Cy3–Cy5 labeled DNA, in the absence (green) and presence (orange) of yNhp6A. These spectra were used in the calculation of the acceptor ratio Υ, as detailed in Supplementary Methods 1.6. The measured emission intensities were first corrected for distortions arising from 'inner-filter' effects attributed to different optical densities of the sample at the donor and acceptor excitation wavelengths (43,44), as outlined in Supplementary Methods 1.6 and Supplementary Figure S2. The acceptor ratio method to monitor FRET is preferable over the donor fluorescence method because the latter requires the ratio of fluorescence intensities from measurements on two separate samples, single-labeled and double-labeled, which introduces additional errors from uncertainties in the sample concentrations. To convert acceptor ratio to FRET efficiency requires knowledge of the extinction coefficients of the donor and acceptor fluorophores at the two different excitation wavelengths, and accurate estimates of labeling efficiency. Here, we are interested primarily in how these values change with varying ionic conditions and temperature and therefore restrict ourselves to acceptor ratio measurements as a measure of FRET efficiency for the results reported below.

Both yNhp6A–DNA complex stability and DNA bending decrease with increasing salt concentration

We first determined protein–DNA binding stoichiometry, the active protein concentration, and the binding affinity of yNhp6A for unlabeled DNA at 25°C and at different salt concentrations. Electrophoretic gel mobility shift assays and direct measurements of on- and off-rates by biolayer interferometry (BLI) were performed as described in Materials and Methods and in Supplementary Methods 1.3 and 1.4. Electrophoresis is ideal for detection of higher-order protein–DNA complexes that can form with sequence-nonspecific proteins such as yNhp6A, so was used to define binding conditions where 1:1 complexes predominated. These measurements demonstrated evidence for more than one protein binding to DNA at conditions of protein excess in 100 mM NaCl. Higher-order complexes were less prevalent in 200 mM NaCl (Supplementary Figure S3). BLI is uniquely powerful in determining kinetics for complex formation and decomposition under different salt conditions. These measurements yielded equilibrium dissociation constant (K_D) values of 74.1 ± 1.4 nM, 795 ± 15.5 nM and 1.91 ± 0.15 μM at 100 mM, 200 mM and 300 mM NaCl, respectively (Supplementary Figure S4). The data thus revealed that yNhp6A–DNA complex stability decreases with increasing concentration of NaCl. This destabilization of a protein–DNA complex by increasing salt concentration is expected for any binding process involving cation release (23,33,40).

To confirm active protein concentration estimates under equilibrium FRET conditions, we performed titration studies measuring acceptor ratio versus protein concentration at each salt condition using 5 μM DNA (Figure 3B), and fitted the binding isotherms using the above K_D values and a scale factor that accounted for any inactive fraction of protein in our samples. These measurements yielded active protein concentrations at 100 mM and 200 mM NaCl that were within 10% of the estimates from binding studies (Supplementary Figure S5). Interestingly, these data suggest that the extent to which the DNA is bent in the complex decreases with increasing salt, with Υ_C (the acceptor ratio of the complex under saturating conditions) of 0.245 ± 0.001 at 100 mM NaCl, 0.212 ± 0.001 at 200 mM NaCl and 0.180 ± 0.011 at 300 mM NaCl. This indication of a [salt]-dependent increase in the relative population of unbent versus bent DNA conformation within an apparently intact protein–DNA complex is reminiscent of a previous report for related proteins (23), as well as a recent report for IHF (45). Evidence that the protein–DNA complex remains intact under these conditions is discussed below. We note here that the titration data at 300 mM NaCl did not reach saturation even with 4-fold excess of protein and therefore the active protein concentration and corresponding Υ_C were less well determined at this salt condition.

yNhp6A protein is stabilized against thermal denaturation by DNA binding

To examine the temperature range over which yNhp6A protein remains folded, we performed thermal denaturation studies of yNhp6A in the absence and presence of DNA, using far-UV CD measurements (Supplementary Figure S6). Thermal denaturation profiles reveal that isolated yNhp6A exhibits a melting temperature of 41.7 ± 1.5°C, independent of [NaCl]. In contrast, in the presence of sufficient DNA to bind all yNhp6A molecules, the protein unfolding transition is shifted to higher temperatures, occurring at 66.1 ± 0.7°C in 100 mM NaCl, 54.4 ± 1.0°C in 200 mM NaCl, and 48.2 ± 0.1°C in 300 mM NaCl. Furthermore, the melting profiles from CD spectroscopy were found to be completely reversible, indicating reversibility of conformational changes in the protein as a result of thermal denaturation (Supplementary Figure S7). This result is important for the T-jump studies reported here that require multiple heating/cooling cycles for data acquisition at each temperature. The result is not unexpected as reversible yNhp6A folding is well known and, in fact, is exploited in purifying the recombinant protein from *E. coli*. CD measurements also indicate that there is already a 10% change in free protein conformation at ∼30°C (Supplementary Figure S6A and B), while in the presence of DNA this conformational change is less than 10% up to ∼55°C in 100 mM NaCl, ∼45°C in 200 mM NaCl and ∼35°C in 300 mM NaCl (Supplementary Figure S6C–H). We therefore conclude that the protein:DNA complex remains largely intact up to the above-mentioned temperatures at each of the salt conditions. Further studies were conducted only at physiologically-relevant NaCl concentrations of 100 and 200 mM because of the propensity of the protein to dissociate and unfold at 300 mM NaCl even at low temperatures.

Increasing temperature induces DNA unbending prior to yNhp6A–DNA complex dissociation

To explore evidence for a complex of yNhp6A with straightened DNA, we examined how FRET in the yNhp6A–DNA complex depends on temperature. Figure 4 shows the acceptor ratio (Υ) as a function of temperature measured for Cy3–Cy5 labeled DNA (20 μM) in the absence and presence of protein (28 μM). In 100 mM NaCl, the data show that for free DNA, Υ decreases nearly monotonically from 0.121 ± 0.002 to 0.044 ± 0.002 as the temperature is raised from 15 to 75°C. Above ∼75°C there is a sharp drop in Υ, indicating a structural transition in the DNA. Similar behavior is seen at 200 mM NaCl. We suppose that this structural transition is the separation of the two DNA strands upon DNA melting. When DNA strands are completely separated, FRET efficiency between the dyes is expected to drop to zero. A non-zero acceptor ratio value at the highest temperature in these measurements is attributed to some direct excitation of the acceptor even at wavelengths where the donor is excited.

Acceptor ratio versus temperature measurements in the presence of yNhp6A were performed with 28 μM protein and 20 μM DNA. At this protein:DNA ratio, assuming ∼93% active protein concentration as determined by the titration studies (Figure 3B and Supplementary Figure S5), we expect ∼99% complex in 100 mM NaCl and ∼91% complex in 200 mM NaCl. For 20 μM DNA in the presence of 28 μM yNhp6A we observed increased Υ values at 15°C: 0.253 ± 0.002 at 100 mM NaCl and 0.189 ± 0.001 at 200 mM NaCl, consistent with higher FRET as a result of DNA bending in the complex (Figure 4A and B). As the tempera-

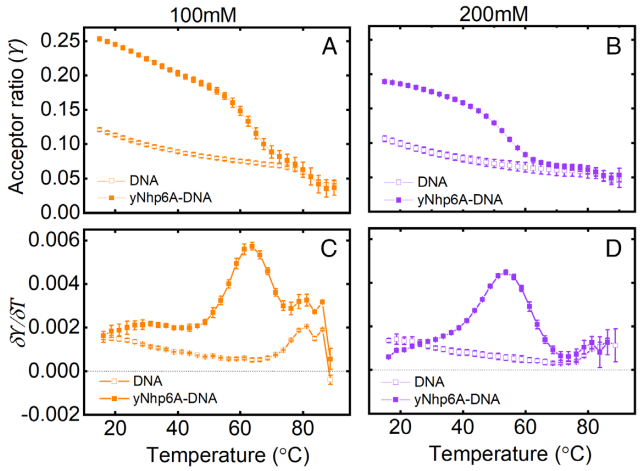

Figure 4. Temperature dependence of acceptor ratio on Cy3–Cy5-labeled DNA, with and without yNhp6A. (**A, B**) The equilibrium acceptor ratio (Υ) values for Cy3–Cy5-labeled DNA (open squares) and yNhp6A–DNA complex (filled squares) are plotted as a function of temperature for measurements in (A) 100 mM NaCl and (B) 200 mM NaCl. Measurements were done with 20 μM DNA and 28 μM yNhp6A. (**C**, **D**) The first derivative of acceptor ratio with respect to temperature ($\delta\Upsilon/\delta T$) are plotted for DNA only (open squares) and yNhp6A–DNA complex (filled squares) in (C) 100 mM NaCl and (D) 200 mM NaCl.

ture was raised, Υ decreased in both 100 and 200 mM NaCl. Two distinct transitions were observed, as illustrated in the corresponding derivative plots (Figure 4C and D). We hypothesize that the first prominent transition (∼62°C in 100 mM NaCl and ∼52°C in 200 mM NaCl) has contributions from both DNA unbending in the intact DNA–yNhp6A complex (a unimolecular process) and from the dissociation of DNA from the protein (a bimolecular process); the second transition (above ∼75°C) is attributable to melting of free DNA after protein dissociation, similar to what we observe in DNA-only measurements. Importantly, *we observe decreases in FRET acceptor ratio at temperatures below the first transition*. We hypothesize that these decreases reflect DNA unbending in the absence of complex dissociation. Consistent with these conclusions, acceptor ratio measurements in 100 mM NaCl at two different protein:DNA concentrations (7 μM:5 μM and 28 μM:20 μM) revealed concentration-independent change in Υ up to ∼40°C; with further increase in temperature, a clear deviation was observed between the measurements at the two concentrations as expected for bimolecular dissociation (Supplementary Figure S8). Additional anisotropy experiments over the same temperature range further support this conclusion, as detailed below.

To rule out any artefactual results from not fully complexed DNA in 200 mM NaCl, we also compared acceptor ratio measurements with 40 and 60 μM protein (2-fold and 3-fold excess, respectively), predicted to yield ∼96% and ∼98% complex, respectively (Supplementary Figure S9). Although increasing protein concentration did increase the fraction complex and hence the acceptor ratio values at the low temperature end, the overall shape of the temperature-dependent behavior remained unchanged except that the complex dissociation transition shifted to higher temperatures as anticipated. Conditions close to 1:1 complex were preferred for subsequent equilibrium studies because of evidence from electrophoretic gel mobility shift studies of formation of higher-order protein–DNA complexes when protein was in excess of DNA, as noted above.

Anisotropy measurements monitor yNhp6A–DNA complex dissociation

To further distinguish unimolecular unbending of DNA within the yNhp6A–DNA complex (a prediction of the hypothetical bind-then-bend mechanism) from the bimolecular yNhp6A–DNA dissociation process, we measured yNhp6A–DNA complex stability by steady-state fluorescence anisotropy across the same range of temperatures and [NaCl] as in the FRET acceptor ratio measurements. Anisotropy is a measure of the molecular tumbling rate, which in turn depends on the rotational diffusion constant and hence on the shape and size of the molecule or complex of interest. We expect a smaller anisotropy value (more rapid rotational dynamics) for DNA alone compared to the yNhp6A–DNA complex. An even smaller anisotropy value is expected for single-stranded DNA after duplex denaturation.

The sensitivity of the anisotropy measurements to monitor complex formation was validated by titration measurements at 100 and 200 mM NaCl with 5 μM Cy5-labeled DNA and increasing protein concentrations (Supplementary Figure S10). These measurements detected complex formation and confirmed that more than one yNhp6A protein can bind to the DNA duplex at protein stoichiometries in excess of 1:1, particularly at 100 mM NaCl. These results corroborate electrophoretic gel mobility shift studies in two ways. First, while anisotropy measurements in both salt conditions followed an apparent 1:1 binding isotherm, the change in anisotropy values between free DNA and yNhp6A–DNA complex was larger in 100 mM NaCl (0.266 ± 0.003 to 0.305 ± 0.002) than in 200 mM NaCl (0.266 ± 0.002 to 0.288 ± 0.002). Second, the apparent fraction of active protein determined from the fits to 1:1 binding isotherms was only ∼49% in 100 mM and ∼78% in 200 mM compared with ∼93% in both salt conditions obtained from the corresponding acceptor ratio titration studies (Supplementary Figure S5). These data confirm that protein excess can lead to more than one protein binding to each DNA duplex, particularly in 100 mM NaCl. It is possible that two proteins bind per DNA under saturating conditions. Higher-order protein–DNA complexes were less stable in 200 mM NaCl.

In light of these results, we performed temperature-dependent anisotropy measurements near the 1:1 condition (28 μM:20 μM protein:DNA) at both 100 mM and 200 mM NaCl. To collect a comprehensive set of data, we performed independent anisotropy measurements on single-stranded DNA ($r_{S,exp}$), duplex DNA ($r_{D,exp}$) and DNA in complex with yNhp6A ($r_{C,exp}$) as a function of temperature (Figure 5). The anisotropy of single-stranded DNA, $r_{S,exp}$, was found to be 0.246 ± 0.004 at 100 mM NaCl and 15°C. This value gradually decreased with increase in temperature and then plateaued at about 80°C (Figure 5A). The temperature-dependent decrease in $r_{S,exp}$ is at-

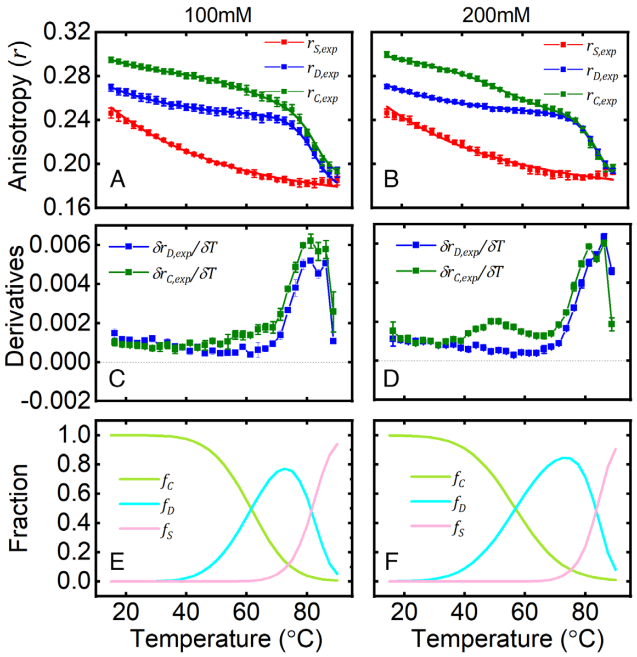

Figure 5. Fluorescence anisotropy measurements on Cy5-labeled DNA and yNhp6A–DNA complex. (**A**, **B**) Steady-state anisotropy values, measured for single DNA strand ($r_{S,exp}$: red), duplex ($r_{D,exp}$: blue) and complex ($r_{C,exp}$: green) are plotted as a function of temperature for measurements at (A) 100 mM NaCl and (B) 200 mM NaCl. Measurements were done with 20 μM DNA and 28 μM yNhp6A. Continuous lines are fits to the anisotropy profiles using the global modeling approach as described in Supplementary Methods 1.9. (**C**, **D**) The first derivative of the anisotropy with respect to temperature of complex ($\delta r_{C,exp}/\delta T$: green) and duplex ($\delta r_{D,exp}/\delta T$: blue) are plotted as a function of temperature for measurements in (C) 100 mM NaCl and (D) 200 mM NaCl. (**E**, **F**) The fractions of DNA in complex (f_C: lime green), free duplex (f_D: cyan) and free single-stranded (f_S: pink), as obtained from the global modeling of the yNhp6A–DNA complex anisotropy, are plotted as a function of temperature for measurements in (E) 100 mM NaCl and (F) 200 mM NaCl.

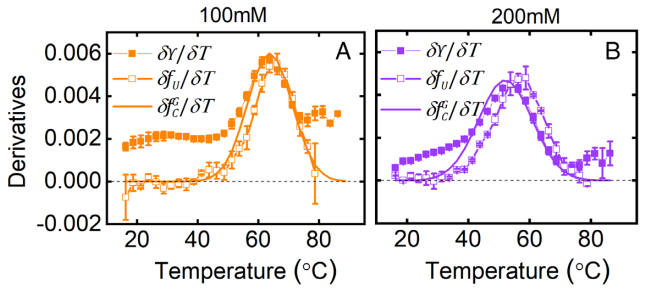

Figure 6. Derivatives of acceptor ratio (Υ), fraction of complex (f_C), and fraction unfolded (f_U) with temperature. (**A**, **B**) The first derivative with respect to temperature of acceptor ratio ($\delta\Upsilon/\delta T$, filled squares), and fraction unfolded from CD measurements ($\delta f_U/\delta T \times 0.1$, open squares) are plotted as a function of temperature for measurements in (A) 100 mM NaCl and (B) 200 mM NaCl. The continuous lines are proportional to the derivative of the fraction in complex as deduced from Gaussian fits to the complex anisotropy derivatives (Supplementary Figure S11), denoted as $\delta f_C^G/\delta T$ (× 18 for 100 mM and × 8 for 200 mM salt).

tributed to a decrease in the effective persistence length of ssDNA with increasing temperature (likely arising from disruption of stacking interactions within single-stranded DNA) and hence a decrease in its radius of gyration (46). The anisotropy of duplex DNA, $r_{D,exp}$, at 15°C was 0.269 ± 0.003, higher than $r_{S,exp}$, as expected, and for the complex sample, $r_{C,exp}$, it was even higher (0.295 ± 0.002). The measured values of $r_{S,exp}$ and $r_{D,exp}$ are in good agreement with reported values in the literature for Cy3-labeled single-strands and duplex DNA of similar length (47). As the temperature was increased, both $r_{D,exp}$ and $r_{C,exp}$ decreased. This change was initially gradual, but then more rapid above ∼70°C. The initial gradual decrease in $r_{D,exp}$ and $r_{C,exp}$ is attributed to an intrinsic decrease in the anisotropy of the duplex and complex species, respectively. The sharp decrease in $r_{D,exp}$ at higher temperatures is attributed to melting of duplex DNA into single-stranded components, while the decrease in $r_{C,exp}$ is attributed to (i) dissociation of DNA from the protein as the temperature is raised and (ii) at still higher temperatures, melting of the dissociated DNA. At the highest temperatures in these measurements, $r_{S,exp}$, $r_{D,exp}$ and $r_{C,exp}$ converge, indicating complete dissociation of DNA from the protein, accompanied by DNA melting.

In 200 mM NaCl, complex dissociation is better separated from DNA melting, with the two transitions more clearly evident in the temperature dependence of $r_{C,exp}$ (Figure 5B).

Changes in $r_{D,exp}$ and $r_{C,exp}$ are better visualized in the derivative plots, $\delta r_{D,exp}/\delta T$ and $\delta r_{C,exp}/\delta T$ (Figure 5C and D). In 100 mM NaCl complex dissociation appears as a shoulder in the plot of $\delta r_{C,exp}/\delta T$ versus temperature at ∼60°C, followed by DNA melting, with a peak ∼80°C. In 200 mM NaCl, the derivative $\delta r_{C,exp}/\delta T$ shows two clear peaks, one ∼50°C (attributed to complex dissociation) followed by DNA melting at ∼85°C. To separate the two transitions, we fitted the complex anisotropy derivatives $\delta r_{C,exp}/\delta T$ as the sum of two Gaussian components (Supplementary Figure S11), and assigned the first Gaussian as reflecting complex dissociation and the second one as reflecting DNA melting. As a control, we also made anisotropy measurements at a higher (60 μM:20 μM) protein:DNA ratio (Supplementary Figure S12). In 100 mM NaCl, the 3-fold excess protein condition exhibited anomalous behavior with an apparent transition appearing below ∼50°C. We attribute this to binding of multiple proteins per DNA. No such anomaly was observed in the 200 mM NaCl, consistent with less interference from higher-order complexes in higher salt.

Separating the temperature range for DNA unbending from dissociation of the yNhp6A–DNA complex

To confirm that straightened DNA can be detected in complex with Nhp6A, we combined the information on DNA shape (complex acceptor ratio, Υ), yNhp6A–DNA complex stability (anisotropy), and protein stability (CD). We compared the temperature derivatives of the acceptor ratio ($\delta\Upsilon/\delta T$), the fraction of intact complex (first Gaussian component of fits to the derivatives of complex anisotropy), and fraction of unfolded protein ($\delta f_U/\delta$T; from CD data), as shown in Figure 6. Three key observations are evident. First, temperature derivatives of the fraction unfolded (from CD) overlapped remarkably with the first Gaussian component (derivative of complex anisotropy), lending support to our conclusion that yNhp6A is stabilized against

thermal denaturation while bound to DNA, and that complex dissociation and protein unfolding occur in a concerted manner under these conditions. Second, complex dissociation transitions (from anisotropy and CD) overlapped with the dominant peak of the temperature derivative of the acceptor ratio ($\delta\Upsilon/\delta T$), measured under identical conditions. Third, and most importantly, DNA unbending, as detected by $\delta\Upsilon/\delta T$, was already evident below ∼45°C in 100 mM NaCl and below ∼35°C in 200 mM NaCl. These are temperature ranges over which no dissociation of DNA from the complex was detected by changes in anisotropy, $\delta r_{C,exp}/\delta T$, or in fraction unfolded, $\delta f_U/\delta$T (from CD). *These results strongly indicate that DNA unbending occurs within the intact Nhp6A–DNA complex*, especially below ∼45°C in 100 mM NaCl and below ∼35°C in 200 mM NaCl. We therefore conclude that the primary contribution to acceptor ratio changes up to ∼45°C in 100 mM NaCl and ∼35°C in 200 mM NaCl is from unimolecular DNA bending/unbending processes within the intact yNhp6A:DNA complex.

Modeling anisotropy data allows separation of complex dissociation from DNA melting

To further elucidate complex dissociation as a function of temperature, we modeled the temperature dependencies of the anisotropy measurements for the single-stranded, duplex and complex samples ($r_{S,exp}$, $r_{D,exp}$ and $r_{C,exp}$, respectively) in a self-consistent way, using a minimal model in which DNA in the complex samples was assumed to be either free (fully dissociated) or bound, and it was further assumed that free DNA can melt. Three species were thus considered: duplex DNA in complex with protein, free duplex DNA, and single-stranded DNA (fractional populations: $f_C(T)$, $f_D(T)$, and $f_S(T)$, respectively). Two species comprised the DNA-only samples: duplex DNA and single-stranded DNA. While other species may have contributions (e.g. multiple conformations of duplex DNA in protein complex such as straight DNA versus unwound/bent DNA), we expect the largest contributions to the temperature derivative of the anisotropy to come from changes in bound and free DNA populations, and melting of duplex DNA to single-stranded DNA with increased temperature. Anisotropy change due to changes in the shape of the complex are expected to be smaller in comparison. Thus, at each temperature, the measured anisotropies of the duplex DNA and complex samples were described as linear combinations of the fractions: $f_C(T)$, $f_D(T)$, and $f_S(T)$, and the intrinsic anisotropies of each of the species (see Supplementary Methods 1.9). The fractional populations at each temperature were described in terms of two parameters that characterized DNA melting and two additional parameters that characterized complex dissociation (Supplementary Equations S10 and S12). The fits to $r_{S,exp}(T)$, $r_{D,exp}(T)$ and $r_{C,exp}(T)$ obtained from this global analysis are shown in Figure 5A and B. The corresponding fractional populations in the complex samples are shown in Figure 5E and F. The residuals from the fits are shown in Supplementary Figure S13. The resulting temperature derivatives of the fraction complex, $\delta f_C(T)/\delta T$ are in reasonable agreement with the temperature derivative of the fraction complex obtained directly from Gaussian fits to the complex anisotropy

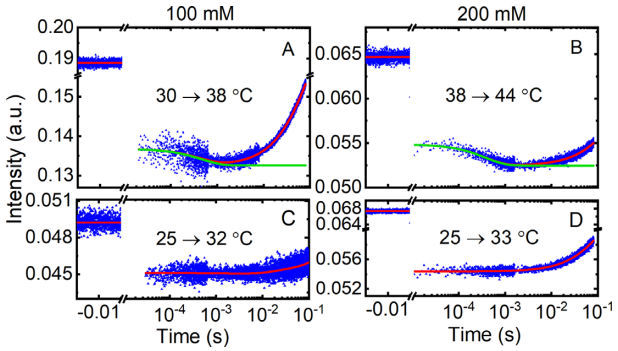

Figure 7. Relaxation traces from T-jump measurements on yNhp6A–DNA complex in 100 mM NaCl. (**A, B**) Fluorescence emission intensity for the yNhp6A–DNA complex, in response to T-jump perturbation, is plotted as a function of time for (A) T-jump from 30°C to 38°C in 100 mM NaCl and (B) 38°C to 44°C in 200 mM NaCl. Negative values are assigned to the time points prior to the infrared laser pulse that induces the T-jump. The continuous red line is a single exponential fit to the observed relaxation kinetics convoluted with the T-jump recovery function (see Supplementary Methods 1.11; Supplementary Equation S18), with relaxation times of 427 μs in (A) and 396 μs in (B). (**C**, **D**) Control experiment on Cy3–Cy5-labeled duplex DNA in the absence of yNhp6A in response to a T-jump from 25°C to 32°C in (C), and from 25°C to 33°C in (D). The continuous lines are a fit to the T-jump recovery function (see Supplementary Equation S17), with characteristic time constants of 185 and 175 ms, respectively. Measurements were done with 20 μM DNA and 28 μM (40 μM) yNhp6A in 100 mM (200 mM) NaCl.

derivatives, as shown in Supplementary Figure S14. Thus, modeling reaffirms our conclusions that the yNhp6A–DNA complex remains mostly intact up to ∼45°C in 100 mM NaCl and up to ∼35°C in 200 mM NaCl, above which we detect complex dissociation.

Dynamics of unimolecular DNA bending/unbending in yNhp6A–DNA complex are measured by laser temperature jump

To gain insight into the dynamics of the DNA bending-unbending equilibrium within intact yNhp6A–DNA complexes, T-jump measurements were performed at 100 and 200 mM NaCl over the entire temperature range at which equilibrium measurements were made. The protein:DNA concentrations for these measurements were 28 μM:20 μM at 100 mM NaCl, and 40 μM:20 μM at 200 mM NaCl, so as to minimize the fraction of free DNA. Typical relaxation traces measured on the Cy3–Cy5-labeled yNhp6A–DNA complex in 100 mM and 200 mM NaCl are shown in Figure 7, together with corresponding control measurements on Cy3–Cy5-labeled DNA duplex in the absence of protein. In all measurements, a continuous wave laser at 530 nm was used to excite the donor (Cy3) molecule and the fluorescence emission intensity of the acceptor (Cy5) was measured as a function of time before and after the arrival of the pulse.

We first describe T-jump measurements on the control (donor-acceptor-labeled DNA only) samples, shown in Supplementary Figure S15a. In these measurements, a sharp drop in the fluorescence emission intensity of the acceptor was observed immediately after the arrival of the infrared pulse that induces the T-jump (defined as t =

0^+ in these kinetics traces). This rapid decrease reflects temperature-dependent decrease in the quantum yield of the donor and acceptor fluorophores as a result of the T-jump, which occurs within the pulse-width of the IR laser pulse (i.e. within 10 ns). The acceptor emission intensity then remained ∼constant until ∼10–20 ms, indicating that the temperature in the heated volume of the sample stays high for that duration. The fluorescence levels eventually decayed back to the pre-laser levels, with a characteristic time constant of 183 ± 6 ms (Supplementary Figure S15b). This slow decay corresponds to the duration of cooling of the heated volume back to the temperature of the surrounding bath such that the sample temperature relaxes back to its initial temperature. This so-called 'T-jump recovery' is well characterized by the functional form of Supplementary Equation S17.

In the presence of yNhp6A (Figure 7A and B), we observed the initial rapid drop in the acceptor intensity in response to the rapid T-jump as well as the slow decay of the T-jump itself, similar to that observed in the corresponding control measurements (Figure 7C and D). However, in addition, in the presence of the protein we observed further decrease in the acceptor emission intensity in the time window of ∼20 μs to ∼10 ms. These relaxation kinetics reflect a change in the population of protein–DNA complexes from the ensemble of conformations representative of the initial (low) temperature to that of the final (high) temperature, resulting in a change in FRET. In yNhp6A–DNA complexes, the DNA unbends when the sample is heated and the distance between the donor and the acceptor fluorophores increases, resulting in a decrease in the FRET efficiency between the fluorophores. Since we monitored the acceptor intensity in our T-jump measurements (with excitation of the donor), a decrease in FRET is reflected in a decrease in the acceptor intensity during this conformational relaxation kinetics, before the temperature of the sample starts to decay back on the longer (∼180 ms) timescale. No such conformational relaxation kinetics in the ∼20 μs to ∼10 ms time window were detected in the control DNA-only samples, as long as the temperature range of these measurements remained well below the melting temperature of the DNA molecule. This confirms that the relaxation kinetics measured in the complex were from yNhp6A-induced DNA conformational changes.

The relaxation kinetics traces in the temperature range 33−68°C in 100 mM NaCl and 44−68°C in 200 mM NaCl were well described in terms of a single-exponential decay convoluted with the 'T-jump recovery' function (Supplementary Equation S18). The relaxation traces and the corresponding residuals from the fits are shown in Figure 7 and Supplementary Figure S16). Relaxation rates and corresponding amplitudes for 100 mM and 200 mM NaCl at different final temperatures are shown in Figure 8. The shape of the amplitudes versus temperature plots are in remarkable agreement with the shape of the $\delta\Upsilon/\delta T$ profiles (Figure 8C and D), confirming that our T-jump studies indeed monitor relaxation kinetics arising from changes in the bent shape of DNA. We note here that although the equilibrium CD measurements show increasing fraction of unfolded protein as the temperature was raised, these CD-detected

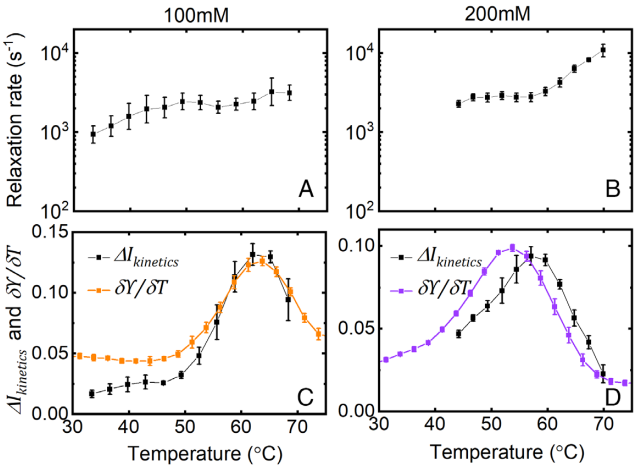

Figure 8. Relaxation rates and relative amplitudes from T-jump measurements on yNhp6A–DNA complex in 100 mM NaCl. (**A**, **B**) Relaxation rates for yNhp6A–DNA complex are plotted as a function of temperature from T-jump measurements in (A) 100 mM NaCl and (B) 200 mM NaCl. (**C**, **D**) The corresponding relative amplitudes in the relaxation kinetics ($\Delta I_{kinetics}$, black squares, calculated as described in Supplementary Methods 1.11; Supplementary Equation S19) are plotted as a function of temperature. Derivatives of the complex acceptor ratio, from equilibrium experiments performed at the same protein:DNA concentrations as the T-jump measurements, are also shown for comparison, in orange squares (C) and purple squares (D).

changes, whether in free protein or in the presence of DNA, were found to be completely reversible (Supplementary Figure S7). Furthermore, the changes in the CD signal in the presence of the DNA are attributed to unfolding of that fraction of the protein that dissociates from the DNA at the higher temperatures. We assert that in the T-jump measurements, the fraction that is already dissociated at the initial temperature, prior to the T-jump, does not contribute to the observed conformational relaxation traces; these kinetics are from the fraction of DNA molecules that still have a protein bound at the initial temperature, but could include contributions from T-jump-induced DNA unbending within the complex as well as T-jump-induced DNA unbending from complex dissociation.

Guided by prior equilibrium studies that revealed a range of temperature where changes in the acceptor ratio Υ for the yNhp6A–DNA complex were detected while the complex remained largely intact, as monitored by both anisotropy and CD changes (Figures 5 and 6), we assign the relaxation kinetics measured in 100 mM NaCl in the temperature range up to 45°C (sample temperature after the T-jump) to *unimolecular bending/unbending of DNA within the intact yNhp6A–DNA complex*. As the temperature of the sample exceeded ∼45°C, the equilibrium studies detected dissociation of the complex, with the dissociated fraction increasing as the temperature was raised. Thus, a T-jump perturbation at these higher temperatures is expected to include contributions from both unimolecular DNA bending/unbending within the intact yNhp6A–DNA complex and bimolecular protein–DNA association/dissociation rates. T-jump measurements at 200 mM NaCl did not reveal any relaxation kinetics in the temperature range expected for the unimolecu-

lar unbending process, likely due to low amplitudes in these kinetics that evaded detection in our apparatus.

Taken together, our equilibrium and kinetics data under physiologically-relevant salt condition of 100 mM NaCl and at temperatures up to ∼45°C support the plausibility of the proposed bind-then-bend kinetic pathway (Figure 2), invoking an intermediate protein–DNA complex involving unbent duplex DNA. The data do not rule out the possibility that the bend-then-bind and/or concerted pathways are also viable (Figure 2).

DISCUSSION

This work set out to address one of three persistent questions concerning the mechanism of HMGB proteins. These questions include understanding intrinsic DNA binding affinities for HMGB proteins, determining whether a static kink or a flexible hinge best describes the properties of deformed DNA in the complex, and establishing the mechanistic order of steps in protein binding and DNA bending. Addressing the third question, we present evidence for the plausibility of the bind-then-bend kinetic pathway (Figure 2) from a combination of FRET-, anisotropy- and CD-based equilibrium and T-jump relaxation kinetics experiments. These experiments do not rule out the other two kinetic paths (bend-then-bind, concerted; Figure 2) as permitted mechanisms.

The bind-then-bend mechanism for a DNA-bending protein was first demonstrated for IHF binding to its cognate H' site, using both stopped-flow and laser T-jump approaches (30,31). The stopped-flow measurements in this case first showed that the unimolecular DNA bending step was distinct from the bimolecular association step (30). Relaxation rates, measured from time-resolved FRET changes when IHF and H' (with FRET labels attached at either terminus) were rapidly mixed together, exhibited a non-linear (hyperbolic) dependence on increasing protein concentration, thus providing strong support for a bind-then-bend mechanism for the IHF-H' complex, and revealing the rate-limiting unimolecular bending step at sufficiently high protein concentration. Equilibrium and T-jump measurements on the IHF-H' complex under identical buffer conditions showed that the complex could be disturbed by T-jump perturbation from a high FRET to a low FRET state, without any bimolecular dissociation (31). These studies enabled direct measurements of unimolecular bending/unbending kinetics and extended the temperature range of observation to much higher temperatures than was accessible by the stopped-flow studies.

Stopped-flow studies on other DNA-bending proteins have had limited success in detecting unimolecular DNA bending steps, suggesting that these kinetics are typically faster than the ∼ms time-resolution of stopped-flow (41,48–50). A notable exception comes from recent stopped-flow measurements of DNA binding and bending by DNA mismatch recognition protein MutS, using anisotropy and FRET measurements as probes of binding and bending (34). These studies also demonstrated a bind-then-bend mechanism for mismatch (T-bulge) recognition by MutS, and revealed DNA bending on timescales of ∼30 ms at 40°C during formation of the specific complex.

While T-jump proved to be a powerful approach for detecting DNA bending/unbending kinetics in the IHF-H' complex on temperature- and time-scales not accessible by stopped-flow, application of this approach to other DNA-bending proteins has been limited by T-jump-induced bimolecular complex dissociation. In these cases, any FRET changes that might arise from DNA unbending are obscured by FRET changes due to complex dissociation. In the present work we address this with a comprehensive approach that circumvents these inherent difficulties in T-jump studies of protein–DNA interaction kinetics. We map the thermodynamic 'phase diagram' for yNhp6a–DNA complex stability as a function of salt concentration and temperature. This effort applied both equilibrium fluorescence anisotropy and FRET as probes of DNA binding and DNA bending, respectively, to interpret subsequent FRET relaxation kinetics measured under these same conditions.

We first address the main conclusions from the equilibrium studies. Our binding isotherms at different salt conditions (measured using acceptor ratio as a probe) demonstrate a decrease in the extent of DNA bending with increasing cation concentration. Why does increasing cation concentration result in DNA straightening within the intact Nhp6A–DNA complex? This observation can be interpreted as a change in the equilibrium constant for the bent-straight DNA conformational equilibrium. By LeChatelier's principle, such a result is expected if the Nhp6A complex with straight DNA binds more monovalent cations than the bent complex. This is plausible if the bent DNA form makes more salt bridges with the protein, releasing more condensed cations than the straight form. Given the known disposition of the N-terminal cationic domain of Nhp6A in the compressed DNA major groove of the bent complex, changes in conformation of protein or DNA that reduce the number of salt bridge contacts in this N-terminal region, for example, are consistent with this result. Other protein conformational transitions driven by cations may have similar consequences for the protein–DNA interface and are also consistent with a shift in the equilibrium toward protein-bound conformations with straight DNA. Indeed, these results are consistent with previous studies that have also shown FRET evidence for partial DNA straightening by increasing salt in the context of intact HMGB protein complexes (23) as well as with intact IHF protein complexes (45).

Our equilibrium results also reveal salt and temperature conditions where DNA unbending within an intact complex is detected. These findings, combined with the T-jump kinetics studies, provide clear evidence for a bind-then-bend pathway describing yNhp6A–DNA interactions, with the first measurement of unimolecular DNA bending rates in the context of a complex with a sequence-nonspecific DNA binding protein. The observed unimolecular DNA bending/unbending kinetics, measured in 100 mM NaCl, are found to occur on timescales of ∼500 μs−1 ms in the temperature range 33−45°C (Figure 9). To put these measurements in the context of measurements on other DNA-bending proteins, we include the corresponding rates measured for the IHF-H' complex, also at 100 mM NaCl (32). While structurally unrelated, both eukaryotic HMGB pro-

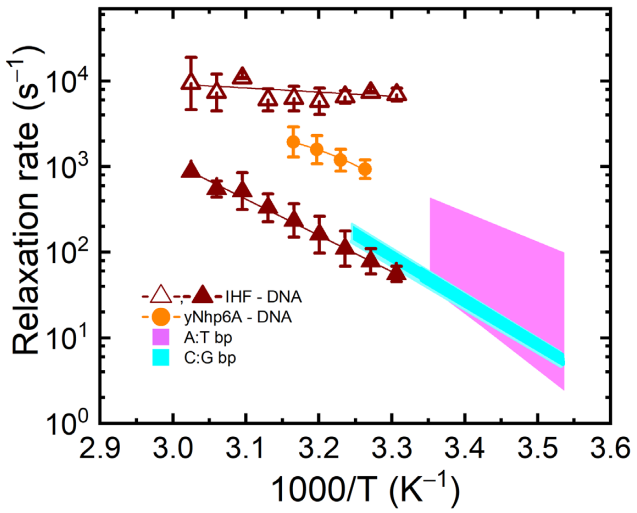

Figure 9. Comparison of unimolecular DNA bending/unbending rates measured on yNhp6A–DNA with those on IHF-DNA. Relaxation rates for the unimolecular DNA bending/unbending kinetics in the yNhp6A–DNA complex measured at 100 mM NaCl (orange circles) are plotted versus inverse temperature. Corresponding rates from biphasic kinetics measured on the IHF-H' complex in 100 mM KCl, from Velmurugu *et al.* (54) are also shown (burgundy, open and filled, triangles). The continuous lines are the corresponding Arrhenius fits. The shaded areas represent the range of base-pair (bp) opening rates from imino-proton exchange measurements for A:T (pink) and C:G (cyan) respectively (63).

teins and *E. coli* IHF bend DNA using amino acid intercalation. HMGB proteins are characterized by two prominent intercalating residues (e.g. methionine and phenylalanine) required to stabilize the bent complex (2,51,52), and IHF has two intercalating proline residues that engage kink sites in the specific complex (53). T-jump studies on specific IHF-DNA complexes and a series of mutants revealed biphasic DNA bending/unbending kinetics (54). The fast phase was attributed to nonspecific bending of DNA by IHF, largely as a result of electrostatic interactions. The slow step was attributed to spontaneous kinking of DNA on time-scales similar to base pair breathing events. The IHF studies indicated that the protein binds randomly to unbent DNA and 'waits' for a spontaneous fluctuation that allows the DNA to sample a distorted conformation that is 'captured' and stabilized by the protein in the target recognition process. The DNA bending/unbending rates measured within the intact yNhp6A–DNA complex fall between the two rates measured for the IHF-H' complex, suggesting that yNhp6A may be actively inducing the DNA bending deformation. However, these data are insufficient to elucidate if the DNA bending step precedes insertion of key intercalating residues or whether the intercalation causes the DNA to bend. These are intriguing questions that are relevant to a wide class of DNA bending proteins, since intercalation of key residues to induce or stabilize sharp kinks in DNA is a common theme in many DNA-bending protein complexes (2,55–58). Answering these questions will require a closer examination of the nature of the intermediates along the DNA bending trajectory, similar to studies on IHF–DNA complexes as well as recent studies carried out to map the sequence of conformational changes during lesion recognition by DNA damage recognition protein, Rad4/XPC, involved in nucleotide excision repair (59,60).

Finally, we address the second question posed initially: does a static kink or a flexible hinge best describe the deformed DNA in a yNhp6A–DNA complex? Prior single molecule FRET studies of Nhp6A lacked the time resolution necessary to clarify whether the bent DNA within the yNhp6A–DNA complex explores two or more states (29). In the present study, it is tempting to interpret the range of FRET signals observed for the yNhp6A–DNA complex at different [NaCl] as direct evidence for a flexible hinge DNA state in the yNhp6A–DNA complex (Figure 3B). Our binding isotherms measured at 20°C demonstrate that FRET signals (as detected by acceptor ratio) under conditions where DNA is saturated with protein clearly decrease with increasing [NaCl], indicating that, on average, DNA in the yNhp6A–DNA complex is less bent at higher [NaCl]. Moreover, our data provide strong evidence for heat-induced unbending within an intact complex. While these data do not prove that there is a distribution of accessible bent conformations at a given [NaCl], they nonetheless support the plausibility of a flexible hinge model. Such dynamic flexibility was recently demonstrated for IHF-DNA specific complexes (45) and has been implicated in the mechanism underlying 'facilitated dissociation' of DNA-binding proteins, whereby dynamic fluctuations in the bound complex enables competitor proteins from solution to bind and displace an already bound protein, resulting in protein concentration dependent dissociation rates (27,61,62).

SUPPLEMENTARY DATA

Supplementary Data are available at NAR Online.

ACKNOWLEDGEMENTS

We thank Mitch Connolly, Evelina Rickeviciute, Jorjethe Roca, and Yogambigai Velmurugu for their immense help and support with equilibrium and T-jump measurements.

FUNDING

National Science Foundation [MCB-1158217 and MCB-1715649 to A.A.]; National Institutes of Health [R01GM75965 to L.J.M.]. The open access publication charge for this paper has been waived by Oxford University Press - *NAR* Editorial Board members are entitled to one free paper per year in recognition of their work on behalf of the journal.
Conflict of interest statement. None declared.

REFERENCES

1. Peters,J.P. and Maher,L.J. 3rd (2010) DNA curvature and flexibility *in vitro* and *in vivo*. *Quart. Rev. Biophys.*, **43**, 23–63.
2. Travers,A.A., Ner,S.S. and Churchill,M.E.A. (1994) DNA chaperones: a solution to a persistence problem. *Cell*, **77**, 167–169.
3. Zimmerman,J. and Maher,L.J. 3rd (2008) Transient HMGB protein interactions with B-DNA duplexes and complexes. *Biochem. Biophys. Res. Commun.*, **371**, 79–84.
4. Rouviere-Yaniv,J. and Gros,F. (1975) Characterization of a novel, low-molecular-weight DNA-binding protein from *Escherichia coli*. *Proc. Natl. Acad. Sci. U.S.A.*, **72**, 3428–3432.

5. Swinger,K.K., Lemberg,K.M., Zhang,Y. and Rice,P.A. (2003) Flexible DNA bending in HU-DNA cocrystal structures. *EMBO J.*, **22**, 3749–3760.
6. Kolodrubetz,D. and Burgum,A. (1990) Duplicated *NHP6* genes of *Saccharomyces cerevisiae* encode proteins homologous to bovine high mobility group protein 1. *J. Biol. Chem.*, **265**, 3234–3239.
7. Paull,T. and Johnson,R. (1995) DNA looping by Saccharomyces cerevisiae high mobility group proteins NHP6A/B. *J. Biol. Chem.*, **270**, 8744–8754.
8. Lu,J., Kobayashi,R. and Brill,S.J. (1996) Characterization of a high mobility group 1/2 homolog in yeast. *J. Biol. Chem.*, **271**, 33678–33685.
9. Merz,K., Hondele,M., Goetze,H., Gmelch,K., Stoeckl,U. and Griesenbeck,J. (2008) Actively transcribed rRNA genes in S. cerevisiae are organized in a specialized chromatin associated with the high-mobility group protein Hmo1 and are largely devoid of histone molecules. *Genes Dev.*, **22**, 1190–1204.
10. Megraw,T.L., Kao,L.R. and Chae,C.B. (1994) The mitochondrial histone HM: an evolutionary link between bacterial HU and nuclear HMG1 proteins. *Biochimie*, **76**, 909–916.
11. Wolffe,A.P. (1999) Architectural regulations and Hmg1. *Nat. Genet.*, **22**, 215–217.
12. Czapla,L., Peters,J.P., Rueter,E.M., Olson,W.K. and Maher,L.J. 3rd (2011) Understanding apparent DNA flexibility enhancement by HU and HMGB architectural proteins. *J. Mol. Biol.*, **409**, 278–289.
13. Murugesapillai,D., McCauley,M., Huo,R., Nelson Holte,M., Maher,L.J., Israeloff,N. and Williams,M.C. (2014) DNA bridging and looping by Hmo1 provides a mechanism for stabilizing nucleosome-free chromatin. *Nucleic Acids Res.*, **42**, 8996–9004.
14. McCauley,M.J., Rueter,E.M., Rouzina,I., Maher,L.J. 3rd and Williams,M.C. (2013) Single-molecule kinetics reveal microscopic mechanism by which High-Mobility Group B proteins alter DNA flexibility. *Nucleic Acids Res.*, **41**, 167–181.
15. McCauley,M., Hardwidge,P.R., Maher,L.J. III and Williams,M.C. (2007) *Optical Trapping and Optical Micromanipulation IV*. 1. SPIE, San Diego, Vol. **6644**, pp. 664405–664412.
16. McCauley,M.J., Zimmerman,J., Maher,L.J. 3rd and Williams,M.C. (2007) HMGB binding to DNA: single and double box motifs. *J. Mol. Biol.*, **374**, 993–1004.
17. McCauley,M., Hardwidge,P.R., Maher,L.J. 3rd and Williams,M.C. (2005) Dual binding modes for an HMG domain from human HMGB2 on DNA. *Biophys. J.*, **89**, 353–364.
18. Becker,N.A., Kahn,J.D. and Maher,L.J. 3rd (2007) Effects of nucleoid proteins on DNA repression loop formation in *Escherichia coli*. *Nucleic Acids Res.*, **35**, 3988–4000.
19. Becker,N.A., Kahn,J.D. and Maher,L.J. 3rd (2008) Eukaryotic HMGB proteins as replacements for HU in *E. coli* repression loop formation. *Nucleic Acids Res.*, **36**, 4009–4021.
20. Becker,N.A. and Maher,L.J. 3rd (2015) High-resolution mapping of architectural DNA binding protein facilitation of a DNA repression loop in Escherichia coli. *PNAS*, **112**, 7177–7182.
21. Crane-Robinson,C., Read,C.M., Cary,P.D., Driscoll,P.C., Dragan,A.I. and Privalov,P.L. (1998) The energetics of HMG box interactions with DNA. Thermodynamic description of the box from mouse Sox-5. *J. Mol. Biol.*, **281**, 705–717.
22. Privalov,P.L., Jelesarov,I., Read,C.M., Dragan,A.I. and Crane-Robinson,C. (1999) The energetics of HMG box interactions with DNA: thermodynamics of the DNA binding of the HMG box from mouse sox-5. *J. Mol. Biol.*, **294**, 997–1013.
23. Dragan,A.I., Read,C.M., Makeyeva,E.N., Milgotina,E.I., Churchill,M.E., Crane-Robinson,C. and Privalov,P.L. (2004) DNA binding and bending by HMG boxes: energetic determinants of specificity. *J. Mol. Biol.*, **343**, 371–393.
24. Masse,J.E., Wong,B., Yen,Y.M., Allain,F.H., Johnson,R.C. and Feigon,J. (2002) The S. cerevisiae architectural HMGB protein NHP6A complexed with DNA: DNA and protein conformational changes upon binding. *J. Mol. Biol.*, **323**, 263–284.
25. Malarkey,C.S. and Churchill,M.E. (2012) The high mobility group box: the ultimate utility player of a cell. *Trends Biochem. Sci.*, **37**, 553–562.
26. Graham,J.S., Johnson,R.C. and Marko,J.F. (2011) Counting proteins bound to a single DNA molecule. *Biochem. Biophys. Res. Commun.*, **415**, 131–134.
27. Graham,J.S., Johnson,R.C. and Marko,J.F. (2011) Concentration-dependent exchange accelerates turnover of proteins bound to double-stranded DNA. *Nucleic Acids Res.*, **39**, 2249–2259.
28. Zheng,G., Czapla,L., Srinivasan,A.R. and Olson,W.K. (2010) How stiff is DNA? *Phys. Chem. Chem. Phys.*, **12**, 1399–1406.
29. Coats,J.E., Lin,Y., Rueter,E., Maher,L.J. 3rd and Rasnik,I. (2013) Single-molecule FRET analysis of DNA binding and bending by yeast HMGB protein Nhp6A. *Nucleic Acids Res.*, **41**, 1372–1381.
30. Sugimura,S. and Crothers,D.M. (2006) Stepwise binding and bending of DNA by *Escherichia coli* integration host factor. *Proc. Natl. Acad. Sci. U.S.A.*, **103**, 18510–18514.
31. Kuznetsov,S.V., Sugimura,S., Vivas,P., Crothers,D.M. and Ansari,A. (2006) Direct observation of DNA bending/unbending kinetics in complex with DNA-bending protein IHF. *Proc. Natl. Acad. Sci. U.S.A.*, **103**, 18515–18520.
32. Vivas,P., Velmurugu,Y., Kuznetsov,S.V., Rice,P.A. and Ansari,A. (2012) Mapping the transition state for DNA bending by IHF. *J. Mol. Biol.*, **418**, 300–315.
33. Vivas,P., Velmurugu,Y., Kuznetsov,S.V., Rice,P.A. and Ansari,A. (2013) Global analysis of ion dependence unveils hidden steps in DNA binding and bending by integration host factor. *J. Chem. Phys.*, **139**, 121927.
34. Sharma,A., Doucette,C., Biro,F.N. and Hingorani,M.M. (2013) Slow conformational changes in MutS and DNA direct ordered transitions between mismatch search, recognition and signaling of DNA repair. *J. Mol. Biol.*, **425**, 4192–4205.
35. Spiriti,J. and van der Vaart,A. (2013) DNA binding and bending by Sac7d is stepwise. *ChemBioChem*, **14**, 1434–1437.
36. Chung,Y.H. and van der Vaart,A. (2014) RevErbalpha preferentially deforms DNA by induced fit. *ChemBioChem*, **15**, 643–646.
37. Peters,J.P., Becker,N.A., Rueter,E.M., Bajzer,Z., Kahn,J.D. and Maher,L.J. 3rd (2011) Quantitative methods for measuring DNA flexibility in vitro and in vivo. *Methods Enzymol.*, **488**, 287–335.
38. Pace,C.N., Vajdos,F., Fee,L., Grimsley,G. and Gray,T. (1995) How to measure and predict the molar absorption coefficient of a protein. *Protein Sci.*, **4**, 2411–2423.
39. Kuznetsov,S.V., Kozlov,A.G., Lohman,T.M. and Ansari,A. (2006) Microsecond dynamics of protein–DNA interactions: direct observation of the wrapping/unwrapping kinetics of single-stranded DNA around the *E. coli* SSB tetramer. *J. Mol. Biol.*, **359**, 55–65.
40. Vivas,P., Kuznetsov,S.V. and Ansari,A. (2008) New insights into the transition pathway from nonspecific to specific complex of DNA with Escherichia coli integration host factor. *J. Phys. Chem. B*, **112**, 5997–6007.
41. Hiller,D.A., Fogg,J.M., Martin,A.M., Beechem,J.M., Reich,N.O. and Perona,J.J. (2003) Simultaneous DNA binding and bending by EcoRV endonuclease observed by real-time fluorescence. *Biochemistry*, **42**, 14375–14385.
42. Clegg,R.M. (1992) Fluorescence resonance energy transfer and nucleic acids. *Methods Enzymol.*, **211**, 353–388.
43. Leese,R.A. and Wehry,E.L. (1978) Corrections for inner-filter effects in fluorescence quenching measurements via right-angle and front-surface illumination. *Anal. Chem.*, **50**, 1193–1197.
44. Kubista,M., Sjoback,R., Eriksson,S. and Albinsson,B. (1994) Experimental correction for the inner-filter effect in fluorescence spectra. *Analyst*, **119**, 417–419.
45. Connolly,M., Arra,A., Zvoda,V., Steinbach,P. J., Rice,P. A. and Ansari,A. (2018) Static kinks or flexible hinges: multiple conformations of bent DNA bound to integration host factor revealed by fluorescence lifetime measurements. *J. Phys. Chem. B*, **122**, 11519–11534.
46. Eisenberg,H. and Felsenfeld,G. (1967) Studies of the temperature-dependent conformation and phase separation of polyriboadenylic acid solutions at neutral pH. *J. Mol. Biol.*, **30**, 17–37.
47. Sanborn,M.E., Connolly,B.K., Gurunathan,K. and Levitus,M. (2007) Fluorescence properties and photophysics of the sulfoindocyanine Cy3 linked covalently to DNA. *J. Phys. Chem. B*, **111**, 11064–11074.
48. Perez-Howard,G.M., Weil,P.A. and Beechem,J.M. (1995) Yeast TATA binding protein interaction with DNA: fluorescence determination of oligomeric state, equilibrium binding, on-rate, and dissociation kinetics. *Biochemistry*, **34**, 8005–8017.
49. Parkhurst,K.M., Brenowitz,M. and Parkhurst,L.J. (1996) Simultaneous binding and bending of promoter DNA by the TATA

binding protein: real time kinetic measurements. *Biochemistry*, **35**, 7459–7465.
50. Huang,S.N. and Crothers,D.M. (2008) The role of nucleotide cofactor binding in cooperativity and specificity of MutS recognition. *J. Mol. Biol.*, **384**, 31–47.
51. Thomas,J.O. and Travers,A.A. (2001) HMG1 and 2, and related 'architectural' DNA-binding proteins (vol 26, pg 167, 2001). *Trends Biochem. Sci.*, **26**, 219–219.
52. Sebastian,N.T., Bystry,E.M., Becker,N.A. and Maher,L.J. (2009) Enhancement of DNA flexibility in vitro and in vivo by HMGB box A proteins carrying box B residues. *Biochemistry*, **48**, 2125–2134.
53. Rice,P.A., Yang,S., Mizuuchi,K. and Nash,H.A. (1996) Crystal structure of an IHF-DNA complex: a protein-induced DNA U-turn. *Cell*, **87**, 1295–1306.
54. Velmurugu,Y., Vivas,P., Connolly,M., Kuznetsov,S.V., Rice,P.A. and Ansari,A. (2018) Two-step interrogation then recognition of DNA binding site by Integration Host Factor: an architectural DNA-bending protein. *Nucleic Acids Res.*, **46**, 1741–1755.
55. Schumacher,M.A., Choi,K.Y., Zalkin,H. and Brennan,R.G. (1994) Crystal structure of LacI member, PurR, bound to DNA: minor groove binding by alpha helices. *Science*, **266**, 763–770.
56. Werner,M.H., Gronenborn,A.M. and Clore,G.M. (1996) Intercalation, DNA kinking, and the control of transcription. *Science*, **271**, 778–784.
57. Gao,Y.G., Su,S.Y., Robinson,H., Padmanabhan,S., Lim,L., McCrary,B.S., Edmondson,S.P., Shriver,J.W. and Wang,A.H. (1998) The crystal structure of the hyperthermophile chromosomal protein Sso7d bound to DNA. *Nat. Struct. Biol.*, **5**, 782–786.
58. Swinger,K.K. and Rice,P.A. (2004) IHF and HU: flexible architects of bent DNA. *Curr. Opin. Struct. Biol.*, **14**, 28–35.
59. Chen,X., Velmurugu,Y., Zheng,G., Park,B., Shim,Y., Kim,Y., Liu,L., Van Houten,B., He,C., Ansari,A. *et al.* (2015) Kinetic gating mechanism of DNA damage recognition by Rad4/XPC. *Nat. Commun.*, **6**, 5849.
60. Velmurugu,Y., Chen,X., Slogoff Sevilla,P., Min,J.H. and Ansari,A. (2016) Twist-open mechanism of DNA damage recognition by the Rad4/XPC nucleotide excision repair complex. *PNAS*, **113**, E2296–E2305.
61. Giuntoli,R.D., Linzer,N.B., Banigan,E.J., Sing,C.E., de la Cruz,M.O., Graham,J.S., Johnson,R.C. and Marko,J.F. (2015) DNA-segment-facilitated dissociation of Fis and Nhp6A from DNA detected via single-molecule mechanical response. *J. Mol. Biol.*, **427**, 3123–3136.
62. Hadizadeh,N., Johnson,R.C. and Marko,J.F. (2016) Facilitated dissociation of a nucleoid protein from the bacterial chromosome. *J. Bacteriol.*, **198**, 1735–1742.
63. Coman,D. and Russu,I.M. (2005) A nuclear magnetic resonance investigation of the energetics of basepair opening pathways in DNA. *Biophys. J.*, **89**, 3285–3292.